THE ROYAL SOCIETY

Received 19 March 2004
Accepted 2 August 2004
Published online 13 December 2004

Gastric flow and mixing studied using computer simulation

Anupam Pal[1], Keshavamurthy Indireshkumar[1], Werner Schwizer[2], Bertil Abrahamsson[3], Michael Fried[2] and James G. Brasseur[1]*

[1]*Department of Mechanical Engineering, 205 Reber Building, The Pennsylvania State University, University Park, PA 16802, USA*
[2]*Department of Gastroenterology and Hepatology, University Hospital, 8091 Zürich, Switzerland*
[3]*AstraZeneca, S-431 83 Mölndal, Sweden*

The fed human stomach displays regular peristaltic contraction waves that originate in the proximal antrum and propagate to the pylorus. High-resolution concurrent manometry and magnetic resonance imaging (MRI) studies of the stomach suggest a primary function of antral contraction wave (ACW) activity unrelated to gastric emptying. Detailed evaluation is difficult, however, *in vivo*. Here we analyse the role of ACW activity on intragastric fluid motions, pressure, and mixing with computer simulation. A two-dimensional computer model of the stomach was developed with the 'lattice-Boltzmann' numerical method from the laws of physics, and stomach geometry modelled from MRI. Time changes in gastric volume were specified to match global physiological rates of nutrient liquid emptying. The simulations predicted two basic fluid motions: retrograde 'jets' through ACWs, and circulatory flow between ACWs, both of which contribute to mixing. A well-defined 'zone of mixing', confined to the antrum, was created by the ACWs, with mixing motions enhanced by multiple and narrower ACWs. The simulations also predicted contraction-induced peristaltic pressure waves in the distal antrum consistent with manometric measurements, but with a much lower pressure amplitude than manometric data, indicating that manometric pressure amplitudes reflect direct contact of the catheter with the gastric wall. We conclude that the ACWs are central to gastric mixing, and may also play an indirect role in gastric emptying through local alterations in common cavity pressure.

Keywords: stomach; gastric motility; lattice-Boltzmann; computer simulation

1. INTRODUCTION

Motility of the stomach is central to proper nutrition, reliable drug delivery, glucose homeostasis with diabetes mellitus, and gastroparesis (Horowitz *et al.* 1994). From a mechanical perspective, the stomach is a mixer, a grinder, a storage chamber and a sophisticated pump that controls the release of aqueous, lipid and solid gastric content into the duodenum (Meyer *et al.* 1994). Whereas many studies have concentrated on gastric motility in emptying (Schwizer *et al.* 1992; Gilja *et al.* 1997; Hausken *et al.* 2002), we focus here on the role of gastric motility in the breakdown of solid particles and mixing of gastric content. We study details of gastric mixing by the coordination of specific patterns of antral contraction with temporal changes in gastric wall motion and pyloric opening, using computer simulations of the human stomach in the fed state.

This study is, to our knowledge, the first application of a numerical model to the study of gastric function. In effect, our computer simulations use Newton's laws of mechanics to extend *in vivo* anatomical data from magnetic resonance imaging (MRI), to details not measurable with current technology in a manner akin to laboratory models, and like laboratory models, the design of the numerical model determines the level of anatomical and physiological detail that can be obtained. Within the bounds of the model, input parameters may be systematically varied to ascertain cause and effect, and to establish sensitivities difficult to obtain with physiological protocols.

2. METHODS

(a) *The numerical method*

We provide here a brief overview of the numerical model used in our study without mathematical or a high level of technical detail. A technical and more detailed description of the numerical algorithm is given in Appendix A.

Our computational model of the human stomach applies a relatively recent advance in numerical methods called the 'lattice-Boltzmann' algorithm that is particularly well suited to fluid flows with complex geometry. A separate numerical model (described below as the 'geometry model') is used to parameterize the time-changing geometry of the gastric lumen that must be provided to the lattice-Boltzmann algorithm as 'boundary conditions'.

The lattice-Boltzmann algorithm, derived from the Boltzmann equation of statistical physics (Chapman & Cowling 1990), describes the movement and interactions of distributions of particles on a mesh that, in our application, encompasses the interior of the stomach and a short segment of duodenum. The great advantage of the lattice-Boltzmann algorithm is the ease with which flows within complex moving boundaries (such as the stomach) can be modelled, and the applicability of the algorithm within massively parallel computer architectures.

Fluid motions within the stomach are generated primarily by the gastric wall motions associated with antral contractile activity, pyloric opening and fundic contraction. It was necessary, therefore, to extend the basic lattice-Boltzmann algorithm to include

*Author for correspondence (brasseur@psu.edu).

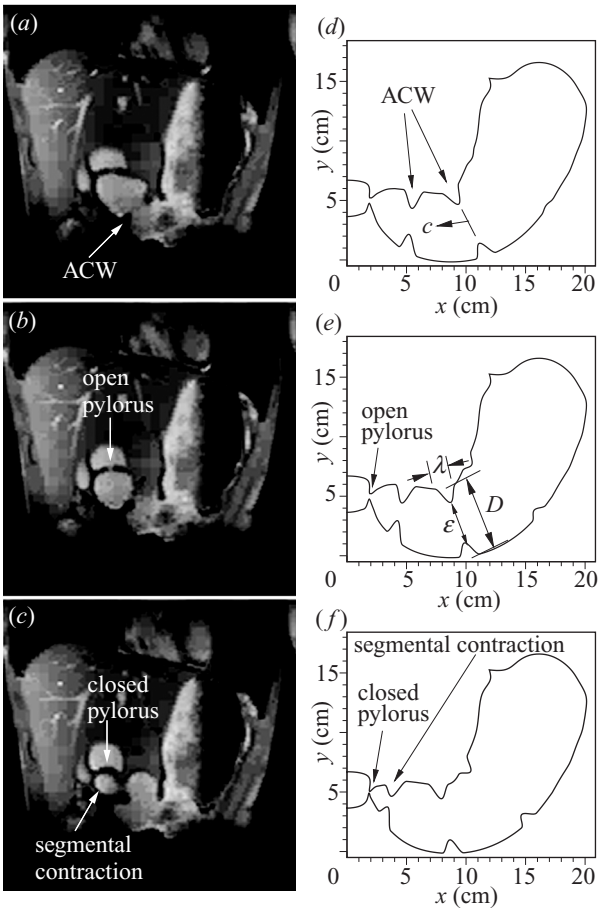

Figure 1. (*a–c*) MRI images from a movie sequence of the human stomach at 4 s intervals. (*d–f*) Stomach geometry model at the same 4 s intervals.

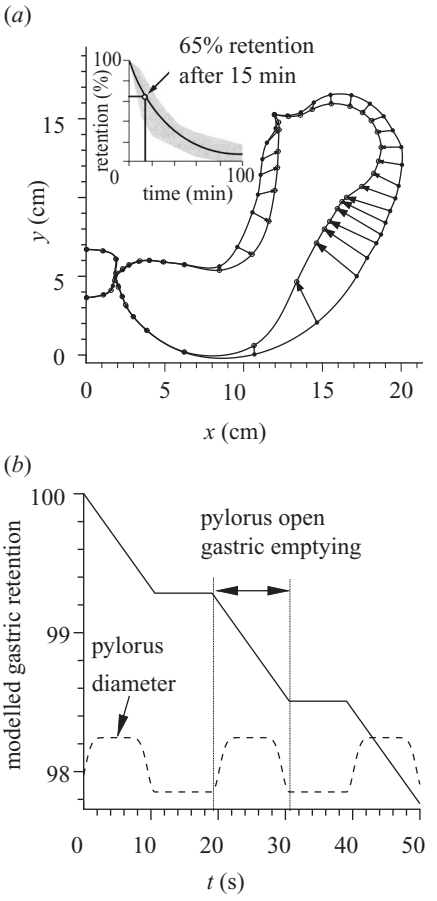

Figure 2. (*a*) Stomach geometry model in the full and partly emptied states. The dots indicate control points through which cubic splice curves were passed to generate the stomach geometry. The arrows show the interpolation path to generate stomach geometry at intermediate times. The inset shows average reduction of liquid nutrient meal (from Horowitz *et al.* 1994) in the human stomach, which is used to parameterize our base model. (*b*) Modelled emptying versus no emptying periods during pyloric opening and closure.

'moving boundary conditions'. We further had to model mathematically the space–time changes in gastric luminal geometry (the 'geometry model' described below) to allow the parameterization and precise control of the boundary conditions in the numerical algorithm. The combined stomach model predicts gastric fluid motions, intragastric pressure, particle dispersion and mixing in the stomach for specified variations in the geometrical characteristics that underlie gastric motility.

(b) *Physiological data*

We made extensive use of MRI of the healthy human stomach filled with 330 ml of a nutrient meal (0.73 kcal ml^{-1}). Figure 1*a–c* show three frames from a typical MRI movie sequence of a healthy volunteer to illustrate the antral contraction wave (ACW) and pyloric opening characteristics captured by the geometry model. The images show coronal views of the stomach tilted to 45° towards the right hand side at 4 s intervals in the fed state. We also compare model predictions of pressure with antral manometric data collected concurrently with MRI as described in Indireshkumar *et al.* (2000) and Faas *et al.* (2001).

(c) *The geometry model*

The geometry of the stomach was modelled in two dimensions (2D) to reduce the high level of complexity in full three-dimensional (3D) models. Previous model studies of peristaltic transport in 2D versus axisymmetric geometries (Brasseur *et al.* 1987; Li *et al.* 1994) show that the 2D model has the same qualitative behaviour as the corresponding 3D model, with modest quantitative differences in pressure and velocity. Most importantly, the fluid motions arising from lumen-deforming muscle contractions are captured by the 2D model.

A realistic geometry model of the stomach was designed from MRI movies of gastric motility, with physiological ranges of anatomical and physiological parameters obtained from the literature. Figure 1*d–f* shows our 'base' geometry model at three time instants corresponding to the MRI sequence in figure 1*a–c*. An ACW initiated in the corpus propagates into the antrum while the pylorus remains closed. While the ACW is in the mid-antrum, the pylorus opens briefly, allowing gastric fluid to empty into the duodenum (figure 1*b* and *e*). When the ACW is within 3 cm of the pylorus, the antral segment between the contraction wave and pylorus contracts segmentally (figure 1*c* and *f*), closing the pylorus (King *et al.* 1984; Pallotta *et al.* 1998). During this terminal antral contraction, the ACW propagates towards the pylorus, continuously reducing the length of the contracting antral segment.

The geometry in figure 1*d–f* was constructed from cubic spline curves (Press 1997) passed through select points (figure 2*a*). From MRI movie we parameterized the timing and location of gastric motility events. In the base model, the width (λ, figure 1*e*) and wave speed (c, figure 1*d*) of the ACWs were 1.8 cm and

2.5 mm s^{-1}, respectively, and ACWs were initiated every 20 s at 14.4 cm from the pylorus. The relative occlusion of the ACW (occlusion diameter to antral diameter without the wave, ε/D, figure 1*e*) decreased linearly from 1 to 0.6 as the ACW propagated for 17.5 s to 10 cm from the pylorus, then remained constant for 16 s. Relative occlusion then decreased linearly for 24 s, reaching 0.1 at the pylorus. Total propagation time and overall pattern of contraction were consistent with the MRI movie, the statistical data of Indireshkumar *et al.* (2000) and the ultrasound results of Pallotta *et al.* (1998).

In this study we simulate gastric motility associated with the emptying of liquid nutrient from a fed stomach. The inset in figure 2*a* indicates that, on average, the stomach empties *ca*. 35% of liquid nutrient content within 15 min after ingestion. Our simulations modelled a linear decrease in volume by 35% in 15 min in the staircase fashion shown in figure 2*b*, with no emptying when the pylorus was closed. In our base model, the pylorus closed when the ACWs were 2 cm from the pylorus, similar to the observations of Indireshkumar *et al.* (2000).

Because our model stomach was filled with incompressible liquid, emptying rate was determined by the specified time changes in gastric volume. Our simulations captured only global emptying. Whereas the sudden reverse flow events across the pylorus reported in the literature (Pallotta *et al.* 1998) were not captured in these simulations, time-local pyloric openings and closings were. As illustrated in figure 2*a*, to control the rate of volumetric change, the shapes and volumes of the stomach were specified in the filled and partly emptied states and linearly interpolated in between.

(d) *The computer simulations*

A uniform grid of typically 300 × 250 cells was placed over the gastric volume. Preliminary numerical experimentation indicated that high accuracy required at least eight grid cells across the narrowest segments at all times. Complete closure was therefore modelled as zero-emptying periods with 1.2 mm pyloric diameter. All simulations assumed a liquid density of 1 g cm^{-3} and a viscosity of 1000 cP.

To explore sensitivity in flow patterns to anatomy and physiology, separate simulations were carried out with the widths of the ACWs increased and reduced by 50% from the base state, and the rate of emptying doubled. Two variations from the base-model ACW occlusion history were explored, one less occlusive (terminal ε/D increased to 0.5) and one more occlusive (ε/D increased to 0.6 at the end of the first phase). To study the importance of motility patterns and antro-pyloric coordination, we simulated the non-physiological situation of a closed pylorus with no emptying while ACWs propagated normally. To evaluate sensitivity to the length of the terminal antral segment, we delayed the time of opening and closure of the pylorus relative to the propagation of the ACWs by 2.9 s, doubling the terminal antral segment length while keeping fixed the pyloric opening period.

(e) *Quantifying gastric mixing*

To quantify mixing, imagine a hypothetical capsule with a large number of small particles suddenly released at specified gastric location at specified time. We define a 'mixing parameter' from the *relative spread* of the particles at short time after release, where 'spread' is quantified by the root-mean-square (RMS) radius, R, of the particles relative to their collective centre of mass,

$$R = \sqrt{\frac{1}{n}\sum_{i=1}^{n}[(x_i - x_c)^2 + (y_i - y_c)^2]}, \qquad (2.1)$$

where (x_i, y_i) are the coordinates of the ith particle and (x_c, y_c) is the centre of mass of the n particles given by mean (x_i, y_i) over all n particles. These particles are small enough to move with, but not alter, the local fluid velocity. After time t, the particles spread from initial RMS radius R_0 to radius R_t. A 'mixing parameter' $M \equiv R_t/R_0 > 1$ defines the level of 'mixing' between time t_0 and t. Particles that have left the stomach are excluded.

3. RESULTS

(a) *Fluid motions in the stomach*

Predicted gastric flow patterns are shown in figure 3 at a time when the pylorus is open and three ACWs coexist. The velocity vectors (figure 3*a*) show that the strongest fluid motions are in the antrum, and two basic antral flow patterns are produced by the propagating ACWs, retropulsive jet-like motions (Code 1970; Schulze-Delrieu & Brown 1985) with the highest velocities (up to 7.5 mm s^{-1}) in the most highly occluded region, and recirculating flow patterns between pairs of ACWs, a ubiquitous feature of all our simulations, and peristalsis in general (Brasseur *et al.* 1987; Li *et al.* 1994). To show clearly the recirculating eddy structure, we show in figure 3*b* the streamlines of gastric fluid flow at a fixed instant in time. ('Streamlines' are lines drawn tangent to velocity vectors, and therefore show the direction of fluid velocity within the stomach at a fixed time.) As shown in the insert, the strength of the eddying motions (defined as the average rotational motion, or 'vorticity', $|\omega_{avg}|$ (Panton 1996), within the eddy) is only significant in antral eddies, and as an ACW approaches the distal antrum, its associated eddies strengthen.

Figure 3*c* quantifies the magnitude of retropulsive jet velocity as an ACW approaches the pylorus. Velocity profiles along the z-axis (figure 3*a*) are shown at 1 s intervals; the maximum retropulsive flow velocity shown on the right as a function of time. The ACW coincides with the z–t locations of maximum retropulsive flow velocity (the dotted line in figure 3*c*). As the ACW propagated distally and became more occlusive, the retropulsive jet strengthened (figure 3*c*) with the most rapid increase and highest jet velocity (7.4 mm s^{-1}) during terminal contraction of the distal antral segment. Contrary to expectations, pyloric closure produced little obvious change in retropulsive flow.

Sensitivities between retropulsive flow velocity and eddying strength with variation in anatomical and physiological parameters of the numerical model are shown in figure 3*d*. Interestingly, retrograde velocity was insensitive to all variations except changes in ACW occlusion. Eddy strength, also, was sensitive to the degree of occlusion of the ACWs and relatively insensitive to differences in coordination between pylorus opening and ACW propagation. Thus, increase or decrease in occlusion ratio is expected to strongly affect antral mixing. Unlike retrograde flow, however, eddy strength was strongly modulated by the width of the ACW, whereas doubling of ACW width had a minimal effect; narrower ACWs produced much stronger recirculating flows, particularly along the lesser curvature wall.

(b) *Comparisons between measured and predicted gastric pressure*

In figure 4 we compare measured with predicted gastric pressure variations. In figure 4*a* manometric pressures recorded at 13 sideholes spaced 3.33 mm through the distal antrum are interpolated and plotted along the catheter axis

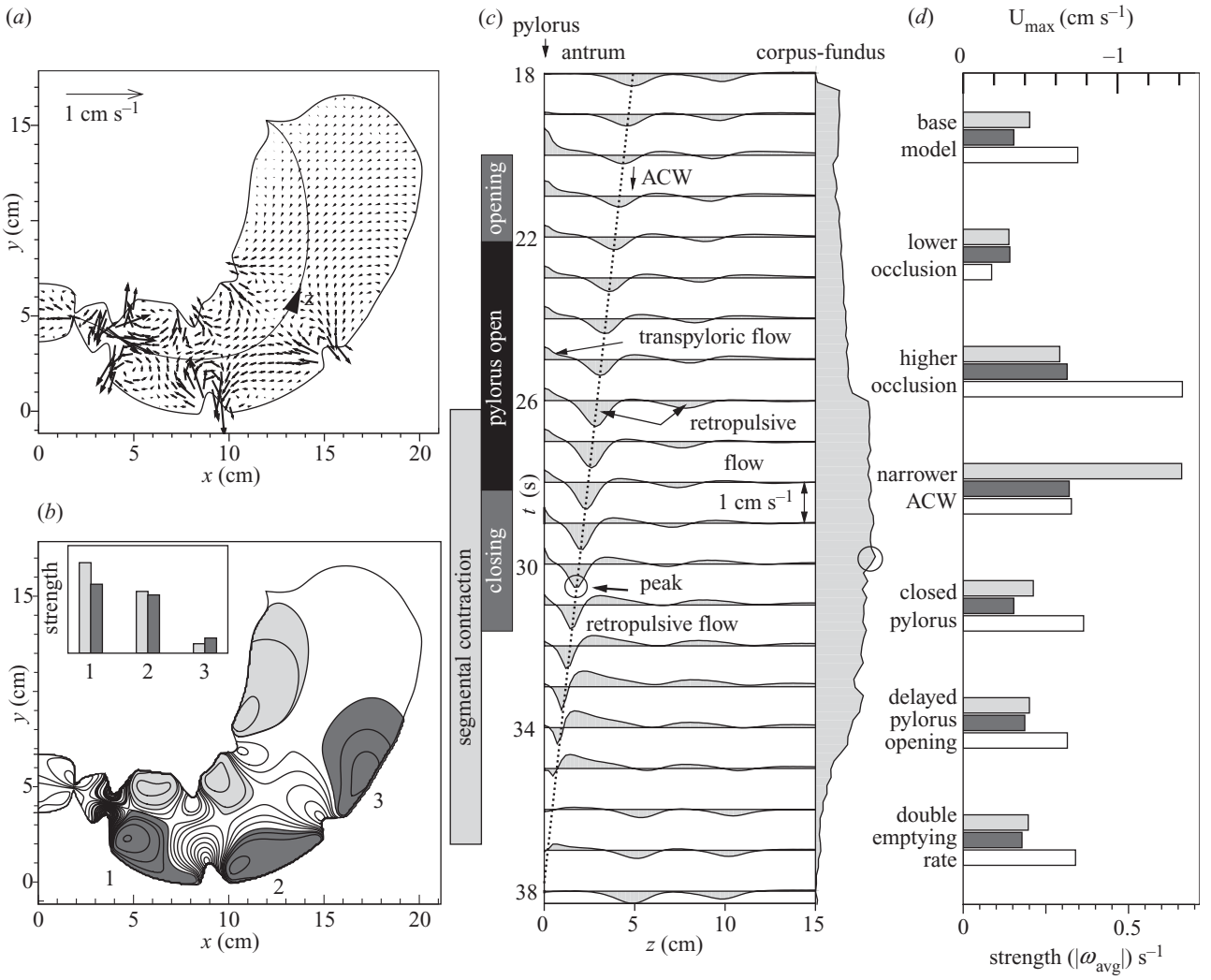

Figure 3. (*a*) Predicted gastric flow velocity vectors at one time instant. (*b*) Instantaneous streamlines (see text for explanation) with three pairs of eddies identified by the shaded areas and labelled 1–3. The insert shows the eddy strengths determined by area averaged vorticity (see text for explanation) magnitude $|\omega_{avg}|$. The lighter and darker grey bars identify eddies on lesser and greater curvature sides respectively. (*c*) Flow velocity along the *z*-axis shown in (*a*), plotted at 1 s intervals. The filled curve on the right is the maximum retropulsive flow velocity through the ACWs as a function of time. The timing of pyloric opening and terminal segmental contraction are shown in the bars on the left. The dotted line follows the propagation of the distal-most ACW in space–time (*z*–*t*). (*d*) Comparison of peak retrograde flow velocities, U_{max} (empty bar) and strengths of the distal-most eddies (light and dark grey bars) between the base model and parametric variations at peak retrograde flow velocity. The grey shading is consistent with (*b*).

at multiple fixed times during the pyloric opening period (Indireshkumar *et al.* 2000). Antral pressures proximal to the pylorus predicted with the base computer model are presented along virtual catheters placed centrally within the lumen (figure 4*b*) and 1 mm from the tip of the ACW on the lesser curvature side (figure 4*d*).

In comparing predicted pressures with measured pressures it is important to appreciate the limitations of each dataset. Whereas manometric pressure variations at 0.5–1 mmHg and below are within the noise level of the instrumentation, higher-magnitude contact pressures from direct squeeze of the lumen wall onto the manometric side-hole are well resolved by perfused manometry (Brasseur & Dodds 1991). By contrast, computer model predications are restricted to gastric fluid pressures; contact pressure cannot be predicted. Thus model predictions of pressure are accurate at low values and difficult to measure accurately by manometry, while manometrically measured contact pressures cannot be captured with the computer model (e.g. the pressure band at the bottom of figure 4*a* that disappears at *ca*. 22.5 s during pyloric opening). However, the space–time structure of ACW-induced pressure variation can be both predicted and measured, albeit with different pressure amplitudes.

Both manometric and simulation data predict an antral peristaltic pressure wave induced by an ACW with overall reduction in pressure proximal to, and enhancement of pressure distal to, the ACW (compare figure 4*a* with *b*,*d*). Furthermore, a pressurization of the terminal antral segment between the ACW and pylorus is apparent in both the physiological and simulation data. The predicted pressures (figure 4*b* and *d*), however, indicate that the antral–duodenal pressure differences associated with average physiological levels of transpyloric liquid flow are only fractions of a mmHg, within the noise level of even the most accurate manometry systems.

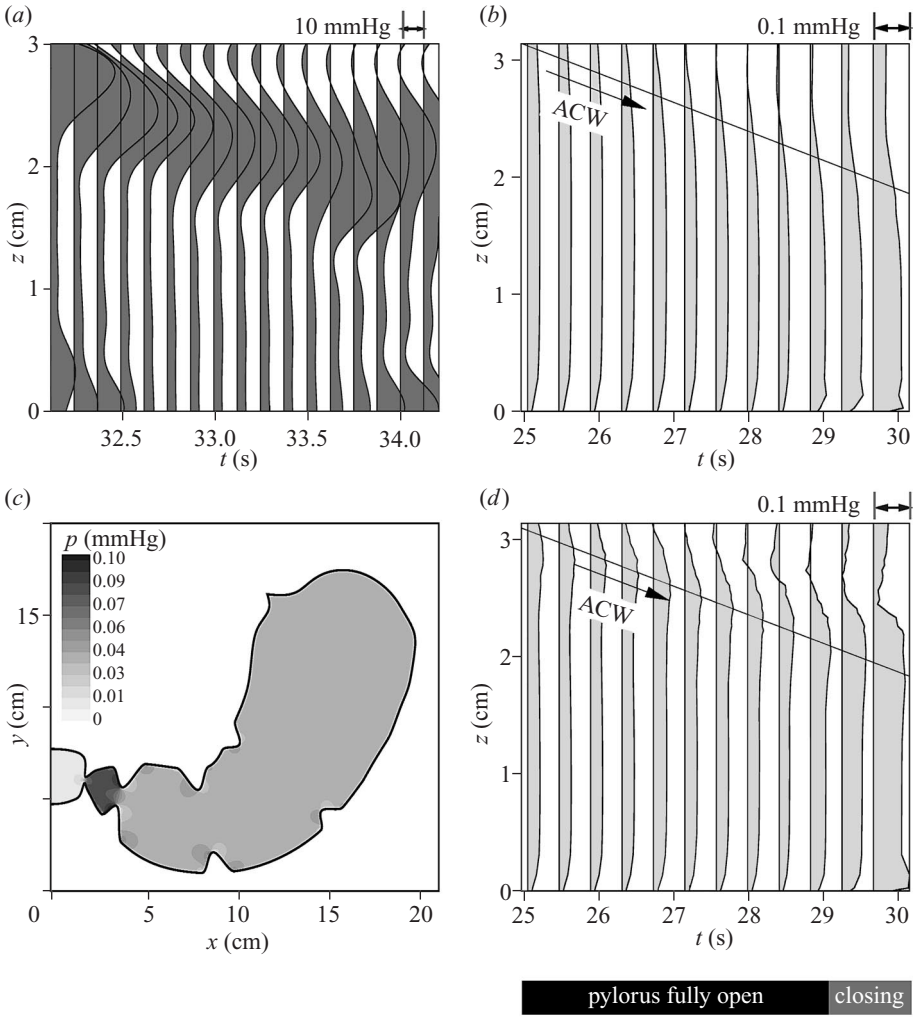

Figure 4. (*a*) Manometric pressure at 13 sensors (spaced 0.33 cm apart) and interpolated spatially at fixed times using cubic splines. Each vertical strip shows luminal pressure variation at fixed times. (*b*) Predicted pressure recorded along a virtual catheter placed centrally through the stomach, plotted similarly to (*a*). (*c*) Greyscale isocontour plot of predicted pressure. (*d*) Predicted pressures recorded along a virtual catheter placed 1 mm from the tips of the ACWs on the lesser curvature side. All pressures were referenced to the proximal duodenum 1 cm from the pylorus.

The simulation shows that pressurization of the terminal antral segment is independent of the location of the catheter (figure 4*b* versus *d*) consistent with the common-cavity nature of pressure there. However, increases in pressure distal to the ACW and reductions in subduodenal pressures proximal to the travelling ACWs are discernible only when the virtual catheter is close to the ACW surface. Furthermore, spatial gradients in pressure are higher in the vicinity of the ACW with the catheter close to the luminal wall (compare slopes of pressure versus z between 2.0 and 3.2 cm in figure 4*b*,*d*). Whereas the computer model predicts a rapid pressure rise (figure 4*d*) similar to manometric data (figure 4*a*), peak manometric pressures measured just distal to ACWs are two orders of magnitude higher than predicted peak pressures, indicating luminal closure in the experimental data during this ACW event. (There is significant variability in measured ACW pressure history.)

Pressurization of the terminal antral segment associated with the advancing ACW and segmental contraction is clear in figure 4*c*. During the initial pressurization period the pylorus is open and gastric emptying occurs in the presence of supra-duodenal pressure just proximal to the pylorus, which can enhance emptying.

(c) *Gastric mixing*

To demonstrate the roles of retropulsive and recirculating flows on mixing we compare in figure 5*a* the locations of simulated particles at an initial time (open circles) with the locations of the same particles after 10 s (filled circles). The retropulsive jet causes the distal-most group of particles to separate, whereas the more proximal recirculating flow transports particles transversely to the gastric wall. Particles in the fundus move towards the antrum in a group with negligible mixing.

The isocontour plot of mixing parameter M in figure 5*b* shows that mixing takes place primarily near the ACW and no significant mixing takes place in the fundus. As ACWs become more lumen-occluding while approaching the pylorus, they become more effective at mixing.

We examine the sensitivity of ACW geometry, pyloric opening and rate of emptying on gastric mixing by plotting in figure 6*a* the mixing parameter averaged over the gastric lumen at the time of strongest retropulsive flow. The base

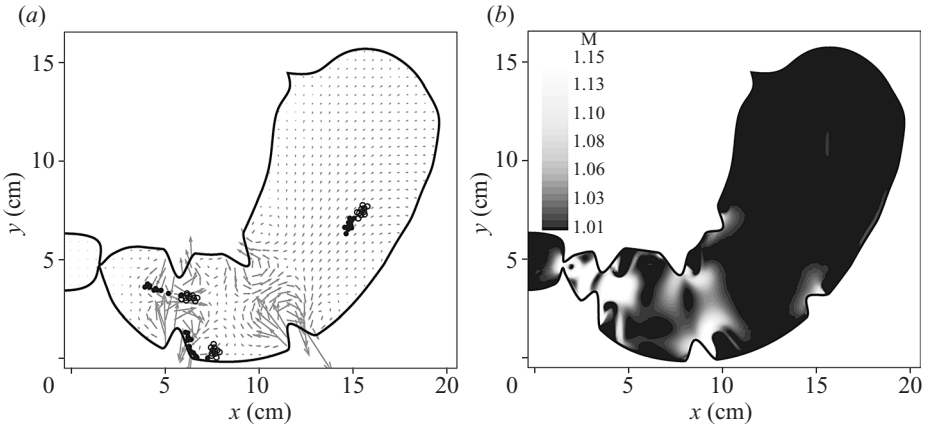

Figure 5. (*a*) Mixing in the stomach illustrated by the spreading of three groups of particles released in different gastric regions from initial locations (open circles) to locations after 10 s (closed circles). (*b*) Greyscale isocontour plot of mixing parameter *M* (calculated over 1 s).

model is the black bar, the grey bars show variations with ACW geometry, and the empty bars indicate other parametric variations. Pyloric closure and rate of emptying have minimal effect on gastric mixing, while changes in ACW occlusion and width affect gastric mixing significantly. More highly occluding and narrower ACWs generate higher rates of mixing.

Figure 6*b–d* illustrates the effects of increased occlusion and reduced width of ACWs relative to the base model. We show five groups of five particles placed initially in different regions of the stomach. The thin lines show the trajectories of each particle over a 2 min period. We observe that particles in the antrum spread relatively rapidly and broadly as compared with particles in the fundus, which mix very little. Dramatic increases in antral mixing occur with higher occlusion and narrower ACWs.

4. DISCUSSION

We have combined Newton's laws of mechanics with MRI to generate new data impossible to obtain experimentally to advance our understanding of gastric motility and mixing. Systematic variation of parameters within a computer model that combined the lattice-Boltzmann numerical method with realistic stomach geometry models revealed previously unknown details of gastric mixing (figures 5 and 6) and related gastric flow patterns (figure 3).

Gastric mixing was found to be limited to the antrum where occluding ACWs generate strong intragastric fluid motions. By contrast, the fundus acts as a reservoir with muscle squeeze that generates slow fluid motions which transport gastric content to the antrum with negligible mixing (figures 5 and 6). Comparing figures 5*b* and 3*a*, *b* leads to the conclusion that two types of wave-induced gastric motion are directly responsible for mixing. High retrograde flow velocities develop in the narrowest antral segment through advancing ACWs (figure 3*a*,*c*) and cause rapid separation of particles (figure 5*a*). The motions of the luminal surface induced by peristaltic contraction waves generate recirculating eddies (figure 3*b*), and mixing is enhanced on the proximal side of the peristaltic contraction (figure 5*b*) as particles follow these induced eddying motions (figure 3*b*). Although maximum retropulsive flow velocities (*ca.* 7.5 mm s^{-1}) are higher than maximum recirculating flow velocities (*ca.* 2 mm s^{-1}), both flow patterns contribute to mixing in complementary ways. Retropulsive flow patterns separate particles longitudinally, while recirculating flow patterns transport particles laterally towards the antral wall. As an ACW approaches the pylorus, the associated axial stretching and the recirculation patterns interact and strengthen (figure 3), enhancing mixing in the distal antrum (figure 6).

Surprisingly, the simulations suggest that the pyloric closure and its timing with ACW propagation play a minor role in the development or strength of retrograde and mixing motions (figure 3). When the pylorus is fully open, the transpyloric flow rate (0.08 $cm^3 s^{-1}$) is only 14% of the flow rate during peak retropulsive velocity through the distalmost ACW (0.58 $cm^3 s^{-1}$) in the base model. A closed pylorus drives all fluid content in the terminal antral cavity proximally, whereas an open pylorus allows some gastric content into the duodenum. The difference in transpyloric versus retropulsive flow rates suggests that pyloric opening influences retrograde flow by at most 10–15%.

Although antral fluid motions and mixing are relatively insensitive to antro-pyloric coordination, the simulations indicated that physiological modulation of wave geometry and occlusion can have a strong effect (figure 6). Specifically, higher occlusion or narrower ACWs strengthen gastric fluid motions and enhance mixing. Furthermore the contraction of the terminal antral segment has a marked influence on retrograde flow velocity (figure 3*c*). Initiation of the terminal antral contraction nearly doubles the retropulsive flow velocity (note the time of 26 s in figure 3*c*) that is sustained well after pyloric closure. Consistent with these results, physiological studies (Hausken *et al.* 1992; Indireshkumar *et al.* 2000) suggest that gastric emptying tends to occur during the period when the ACW is distant from the pylorus and the terminal antrum has not yet initiated segmental contraction. The primary mechanical role of the terminal antral contraction appears to be the generation of strong gastric motions that help separate, break apart and mix gastric content.

However, comparison between predicted and measured intraluminal pressures (figure 4) provides additional detail relevant to gastric emptying and interpretation of manometric pressure. The simulations can resolve pressure variations that are within the noise of manometric data,

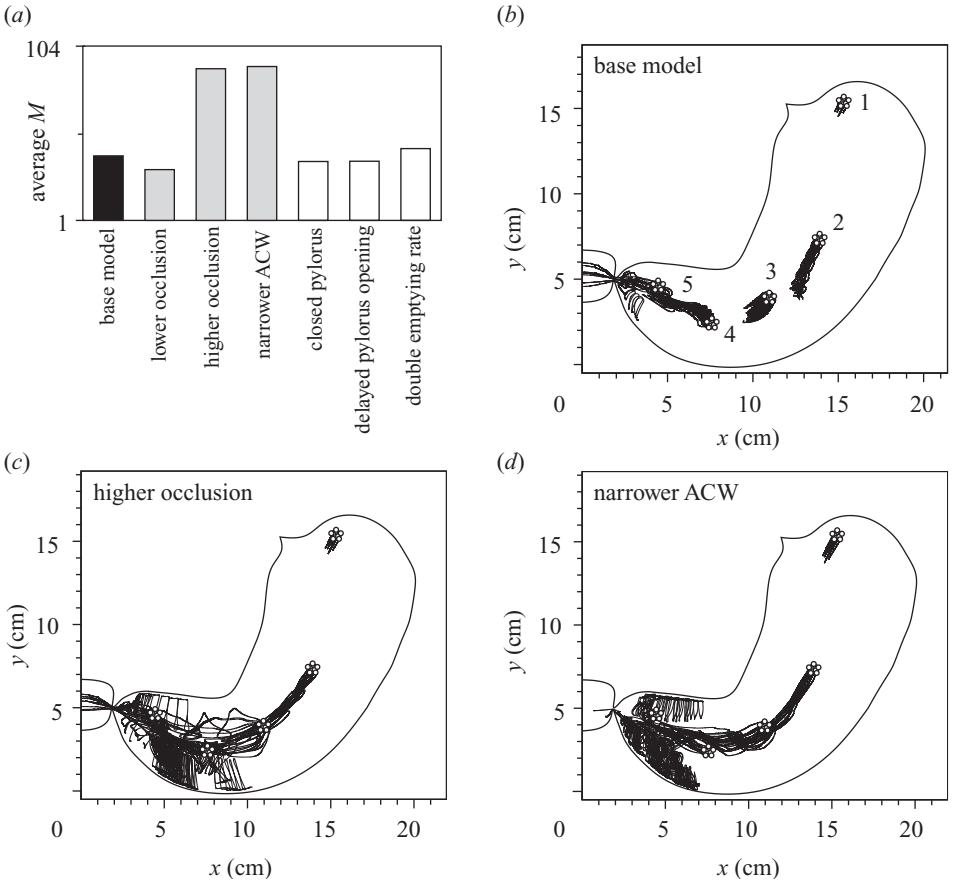

Figure 6. (*a*) Comparisons of mixing parameter averaged over the stomach: the base model (black bar), variations in the ACW geometry (grey bars) and other parametric variations (empty bars). (*b–d*) Enhancement of mixing as a result of variations in ACW geometry, illustrated by comparing the trajectories of five groups of particles released in different gastric regions with the base model (*b*), higher occlusion (*c*) and narrower ACW (*d*).

suggesting that manometry captures primarily higher pressures associated with direct luminal contact. Whereas Hausken *et al.* (2002) report transpyloric pressure differences during emptying in the range 2–20 mmHg, Indireshkumar *et al.* (2000) used high-resolution manometry and conditional statistics to measure mean transpyloric pressure difference of only 0.3 mmHg over 1 cm during antral quiescence and pyloric relaxation. Our computer simulations are consistent with the latter result and suggest that pressure differences of order several mmHg are likely to be a result of direct lumen-occluding contractions over the manometric sidehole.

However, the simulations suggest that the conclusion in Indireshkumar *et al.* (2000), that ACWs make no significant contribution to emptying, may be oversimplified. The numerical model predicts that the antral–duodenal pressure differences associated with average measured levels of transpyloric flow are only fractions of a mmHg. Thus, the slight pressurization of the terminal antral cavity by an ACW still several centimetres from an open pylorus may be sufficient to significantly augment transpyloric flow generated by global common cavity pressure difference between the stomach and duodenum maintained by fundic muscle tone.

This research was supported by AstraZeneca. W.S. was supported by the Swiss National Science Foundation. Early model developments by I.K. were supported by the Janssen Research Foundation. We thank Andreas Steingoetter at University Hospital, Zürich, Switzerland, for the use of his MRI movies of the human stomach.

APPENDIX A

THE LATTICE-BOLTZMANN METHOD

The 'lattice-Boltzmann' numerical method is well suited to predicting fluid flows in complex geometries. The algorithm applies a discretized version of the Boltzmann equation of statistical physics (Chapman & Cowling 1990) to describe the interactions of distributions of microscopic particles on a mesh that, in our application, encompasses the interior of the stomach and a short segment of the duodenum.

The lattice Boltzmann equation is commonly written (Chen & Doolen 1998)

$$f_i(\boldsymbol{x}+\boldsymbol{e}_i\Delta t,t+\Delta t)-f_i(\boldsymbol{x},t)=-(1/\tau)[f_i(\boldsymbol{x},t)-f_i^{\mathrm{eq}}(\boldsymbol{x},t)], \quad \text{(A.1)}$$

where $f_i(\boldsymbol{x},t)$ is the single-particle distribution function at a discretized location $\boldsymbol{x}$ and time t for discretized velocity component $\boldsymbol{e}_i$. $f_i^{\mathrm{eq}}(\boldsymbol{x},t)$ is the equilibrium state towards which the distribution functions relax with time-scale τ (Chen & Doolen 1998). τ is related to fluid kinematic viscosity by $\nu = \frac{1}{2}c_s^2\Delta t(2\tau-1)$, where c_s is the speed of sound in the fluid. Our two-dimensional lattice-Boltzmann simulations apply the '9-speed model' for discretized velocity $\boldsymbol{e}_i$

(Hou *et al.* 1995). Macroscopic fluid density ρ and velocity $\boldsymbol{u}$ are obtained from moments of the distribution function (Chen & Doolen 1998),

$$\rho(\boldsymbol{x},t) = \sum_i f_i(\boldsymbol{x},t),\ \rho(\boldsymbol{x},t)\boldsymbol{u}(\boldsymbol{x},t) = \sum_i f_i(\boldsymbol{x},t)\boldsymbol{e}_i, \tag{A.2}$$

and pressure is given by $p = \rho\, c_s^2$.

MOVING BOUNDARY CONDITION

Gastric wall motions change fluid momentum. We adapt the moving-boundary condition developed by Ladd (1994) and improved by Aidun *et al.* (1998) for solid particles suspended in a liquid. The no-slip condition is enforced by requiring the distribution functions f_i at adjacent nodes to 'bounce back', after streaming to the boundary and after collision, so that

$$f_{i'}(\boldsymbol{x},t_+) - f_i(\boldsymbol{x},t) = -(1/\tau)\left[f_i(\boldsymbol{x},t) - f_i^{\mathrm{eq}}(\boldsymbol{x},t)\right], \tag{A.3}$$

where t_+ is intermediate time between t and $t + \Delta t$, and i' is the inverse lattice direction to i. Ladd (1994) derived an additional contribution from the boundary moving at velocity $\boldsymbol{u}_b$,

$$f_{i'}(\boldsymbol{x},t + \Delta t) = f_i(\boldsymbol{x},t_+) + 6w_{i'}\rho^*\boldsymbol{u}_b \cdot \boldsymbol{e}_{i'}, \tag{A.4}$$

where ρ^* is (Aidun *et al.* 1998)

$$\rho^* = \frac{\sum_i f_i(\boldsymbol{x},t_+)}{1 - \sum_{i'} 6w_{i'}\boldsymbol{u}_b \cdot \boldsymbol{e}_{i'}}, \tag{A.5}$$

and $w_i = 1/9$ for $i = 0$–4, $w_i = 1/36$ for $i = 5$–8. The boundary-induced term in equation (A.4) matches flow velocity ($\boldsymbol{u}$) and boundary velocity ($\boldsymbol{u}_b$) at points halfway between fluid and solid nodes.

As the boundary moves through the fixed lattice, nodes are covered and uncovered. The distribution function of a lattice node transitioning from a solid node to a fluid node is defined by the average over its nearest fluid nodes. To conserve mass, the new distribution function is subtracted from neighbouring distribution functions. By contrast, the distribution functions of fluid nodes that move across the stomach wall to become solid nodes are distributed equally among their nearest fluid nodes.

REFERENCES

Aidun, C. K., Lu, Y. N. & Ding, E. J. 1998 Direct analysis of particulate suspensions with inertia using the discrete Boltzmann equation. *J. Fluid Mech.* **373**, 287–311.

Brasseur, J. G. & Dodds, W. J. 1991 Interpretation of intraluminal manometric measurements in terms of swallowing mechanics. *Dysphagia* **6**, 100–119.

Brasseur, J. G., Corrsin, S. & Lu, N. Q. 1987 The influence of a peripheral layer of different viscosity on peristaltic pumping with Newtonian fluids. *J. Fluid Mech.* **174**, 495–519.

Chapman, S. & Cowling, T. G. 1990 *The mathematical theory of non-uniform gases: an account of the kinetic theory of viscosity, thermal conduction, and diffusion in gases. Cambridge Mathematical Library*. Cambridge University Press.

Chen, S. & Doolen, G. D. 1998 Lattice-Boltzmann method for fluid flows. *A. Rev. Fluid Mech.* **30**, 329–364.

Code, C. F. 1970 New horizons in gastrointestinal physiology. *Arch. Fisiol.* **68**, 1–24.

Faas, H.(and 10 others) 2001 Pressure–geometry relationship in the antroduodenal region in humans. *Am. J. Physiol. Gastrointest. Liver Physiol.* **281**, G1214–G1220.

Gilja, O. H., Detmer, P. R., Jong, J. M., Leotta, D. F., Li, X. N., Beach, K. W., Martin, R. & Strandness Jr, D. E. 1997 Intragastric distribution and gastric emptying assessed by three-dimensional ultrasonography. *Gastroenterology* **113**, 38–49.

Hausken, T., Odegaard, S., Matre, K. & Berstad, A. 1992 Antroduodenal motility and movements of luminal contents studied by duplex sonography. *Gastroenterology* **102**, 1583–1590.

Hausken, T., Mundt, M. & Samsom, M. 2002 Low antroduodenal pressure gradients are responsible for gastric emptying of a low-caloric liquid meal in humans. *Neurogastroenterol. Motil.* **14**, 97–105.

Horowitz, M., Dent, J., Fraser, R., Sun, W. & Hebbard, G. 1994 Role and integration of mechanisms controlling gastric emptying. *Digestive Dis. Sci.* **39** (Suppl. 12), 7S–13S.

Hou, S. L., Zou, Q., Chen, S. Y., Doolen, G. & Cogley, A. C. 1995 Simulation of cavity flow by the lattice-Boltzmann method. *J. Comput. Physics* **118**, 329–347.

Indireshkumar, K.(and 10 others) 2000 Relative contributions of 'pressure pump' and 'peristaltic pump' to gastric emptying. *Am. J. Physiol. Gastrointest. Liver Physiol.* **278**, G604–G616.

King, P. M., Adam, R. D., Pryde, A., McDicken, W. N. & Heading, R. C. 1984 Relationships of human antroduodenal motility and transpyloric fluid movement: non-invasive observations with real-time ultrasound. *Gut* **25**, 1384–1391.

Ladd, A. J. C. 1994 Numerical simulations of particulate suspensions via a discretized Boltzmann-equation. 1. Theoretical foundation. *J. Fluid Mech.* **271**, 285–309.

Li, M. J., Brasseur, J. G. & Dodds, W. J. 1994 Analyses of normal and abnormal esophageal transport using computer-simulations *Am. J. Physiol.* **266**, G525–G543.

Meyer, J. H., Elashoff, J. D., Domeck, M., Levy, A., Jehn, D., Hlinka, M., Lake, R., Graham, L. S. & Gu, Y. G. 1994 Control of canine gastric emptying of fat by lipolytic products *Am. J. Physiol.* **266**, G1017–G1035.

Pallotta, N., Cicala, M., Frandina, C. & Corazziari, E. 1998 Antro-pyloric contractile patterns and transpyloric flow after meal ingestion in humans. *Am. J. Gastroenterol.* **93**, 2513–2522.

Panton, R. L. 1996 *Incompressible flow*. New York: John Wiley & Sons Inc.

Press, W. H. 1997 *Numerical recipes in C: the art of scientific computing*. Cambridge University Press.

Schulze-Delrieu, K. & Brown, C. K. 1985 Emptying of saline meals by the cat stomach as a function of pyloric resistance. *Am. J. Physiol.* **249**, G725–G732.

Schwizer, W., Maecke, H. & Fried, M. 1992 Measurement of gastric emptying by magnetic resonance imaging in humans. *Gastroenterology* **103**, 369–376.

As this paper exceeds the maximum length normally permitted, the authors have agreed to contribute to production costs.